공학석사 학위논문

Sulfur-doped Silicon Oxycarbide by Facile Pyrolysis Process Using Silicon Oil as Anode Materials for Outstanding Performance Lithium Ion Batteries

황 도핑 실리콘 옥시카바이드 합성과 고성능 리튬 이온 배터리 음극소재로의 응용

2020년 12월

서울대학교 융합과학기술대학원

융합과학부 나노융합전공

이 근 호

Sulfur-doped Silicon Oxycarbide by Facile Pyrolysis Process Using Silicon Oil as Anode Materials for Outstanding Performance Lithium Ion Batteries

지도 교수 박 원 철

이 논문을 공학석사 학위논문으로 제출함
2020년 12월

서울대학교 융합과학기술대학원
융합과학부 나노융합전공
이 근 호

이근호의 공학석사 학위논문을 인준함
2021년 1월

위 원 장 김 연 상 (인)

부위원장 박 원 철 (인)

위 원 이 강 원 (인)

Sulfur-doped Silicon Oxycarbide by Facile Pyrolysis Process Using Silicon Oil as Anode Materials for Outstanding Performance Lithium Ion Batteries

Keunho Lee

Program in Nano Science and Technology

Graduate School of Convergence Science & Technology

Seoul National University

Abstract

Silicon oxycarbide (SiOC) attracts soaring attention as an anode material for lithium ion battery due to its outstanding cycle life and unique structure of Si-O-C hybrid bonding. However, poor electrical conductivity is the major drawback of SiOC-based electrodes. In this work, I synthesized sulfur-doped silicon oxycarbide (S-SiOC) via facile pyrolysis from a mixture of commercial silicone oil with 1-dodecanethiol. The as-prepared S-doped SiOC was applied as an anode material for lithium ion battery for the first time. The S doping can improve the electrical conductivity of SiOC by providing extra e^- pathway and accommodate more Li^+ by creating additional reaction sites. The enhanced electrochemical kinetics of Li^+ was verified by Randles-Sevcik equation. For the initial cycle, the electrodes demonstrated a high reversible capacity of 700 mAh g^{-1} at 0.1 A g^{-1} with initial coulombic efficiency of 66.8%. Additionally, the electrodes exhibit a large specific capacity of 378 mAh g^{-1} with a high capacity retention of 84.8%, even after 1000 cycles at 1 A g^{-1}. Therefore, this sulfur-doped silicon oxycarbide with excellent

electrochemical performances has promising potential as an anode material in lihium ion battery.

Keywords: Silicon oxycarbide, Sulfur doping, Anode material, Lithium ion batteries

Student Number: 2019-27948

Contents

List of Figures

1. Introduction

1.1. Lithium ion battteries

Lithium-ion batteries (LIBs) with high energy density, power density and outstanding cycling performance are considered as the most powerful energy storage system (ESS) and have been investigated for a variety of applications such as portable devices and electric vehicles (EVs) [1-4]. Graphite has been widely used and most commercialized as an anodic material in the battery field for some reasons such as low operating potential vs. Li, relatively less volumetric change during cycling, low cost, etc [4, 5]. However, as the demand for the outperforming electronics increases, graphite has faced limitation because of its low theoretical capacity of 372 mAh g^{-1}. For this reason, a large number of studies have been conducted to seeking alternative candidates. Silicon-based anode is one of the most attractive material because of its exceeding theoretical capacity of 3579 mAh g^{-1}. Nevertheless, the problem of large volume change (up to 400 %) during cycling can cause fracture of particles and reduced electrical contact. To alleviate this problem, many novel strategies for Si/C composite materials were adopted [6-8]. In

Si/C composite materials, however, the capacity fading problem is still remained due to the structural breakdown during cycling.

1.2. Silicon oxycarbide

In this context, silicon oxycarbide (SiOC) ceramics recently has drawn attention as an anode material because they can replace carbonaceous and Si-based anodes. SiOCs exhibit thermal and structural stability, good cycle performance, simple synthesis process and high reversible capacity of ~650 mAh g^{-1} which attributed to its unique structure [9]. SiOC ceramics can be represented to $SiO_xC_{4-x} + yC_{free}$ ($0 \leq x \leq 4$), the SiO_xC_{4-x} term stands for Si-O-C glass phase and the yC_{free} term stands for segregated free carbon phase, respectively. The amorphous structure of SiOC ceramics can be obtained by pyrolysis of the polysiloxane-based precursors in an inert atmosphere at a lower temperature (~1100 ^oC) and the structure can be tunable depend on precursors and pyrolysis condition [10]. Recently, silicone oil has been widely used as a precursor of SiOC due to the advantages of low cost and simple synthesis procedure compared to polysiloxane-based precursors [11-16]. Since the first study

about lithium ion storage capability of SiOC ceramics reported by the group of Dahn in 1990s, many pieces of research were conducted for preparing SiOC-based anodes [17-19]. The mechanism of lithium storage in SiOC ceramics was not clear yet and still controversial, but Si-O-C phases and edges of graphene sheets are considered as electrochemically active sites in a lithium storage system [20]. Unfortunately, SiOC-based electrodes generally present inferior charge transfer which results from electrically insulating characteristic and poor ionic transport [9, 21, 22]. To address these issues, various approaches have been used for the SiOC-based electrodes. Many kinds of carbonaceous materials, such as carbon nanotubes [21, 23], carbon nanofibers [24] and graphene [25-27] have been employed as composite materials with SiOC. Also preparing hybrid anodes between SiOC and metal was believed to an effective way of improving electrochemical performance [28, 29]. Kasar *et al*. suggested a stable SiOC/Sn nanocomposite via chemical modifications of two different polysiloxane precursors with tin (II) acetate and pyrolysis process of annealing at 1000 ^{o}C. The prepared SiOC/Sn nanocomposite anode delivered the

capacity of 562 mAh g^{-1} at a current density of 74 mA g^{-1} with little fading over 20 cycles and 133 mAh g^{-1} at a high current rate of 744 mA g^{-1} [29].

1.3. Sulfur doping

Doping can be a notable solution for achieving enhanced electrical conductivity and electrochemical activity. Introduction of heteroatoms (e.g., nitrogen, sulfur, phosphorus) can create active sites and modify electronic structures [30, 31]. In an energy storage system, for example, various carbonaceous materials as anode materials such as graphene, carbon nanotube, and porous carbon have adopted heteroatom doping for their better performances [32-38]. Among them, sulfur has gained attention as a dopant in electrochemical applications due to its atomic radius and smaller electronegativity [39, 40]. Moreover, it can provide extra pathways for electron transfer with C-S-C bonding [41]. H_2S gas atmosphere was generally used as a source of S in doping procedure [42, 43], but it can be dangerous due to its toxicity and flammability.

1.4. Objective

In this work, for the first time, I suggest sulfur-doped silicon oxycarbide (S-SiOC) as an anode material for lithium ion battery. I adopted a sulfur doping strategy for silicon oxycarbide via the facile pyrolysis process of commercial silicone oil with 1-dodecanethiol in an inert atmosphere. I successfully obtained S-doped silicon oxycarbide from mixed liquid precursors without H_2S gas. After pyrolysis, doped sulfur atoms formed covalent bonds with carbon atoms, including partial heterocyclic structure. Sulfur doping can facilitate effective e^- transfer by providing additional pathways of C-S-C bonding and accommodate more Li^+ by supplying additional reactive sites. The as-prepared S-SiOC exhibits remarkable electrochemical performances with a high reversible capacity of 700 mAh g^{-1} with initial coulombic efficiency (ICE) of 66.8%. Furthermore, the electrodes show long cycle stability and excellent rate capability. After 1000 cycles, the electrode delivers 378 mAh g^{-1} with a high capacity retention of 84.8%

2. Experimental Section

2.1 Preparation of SiOC

Bare silicon oxycarbide (SiOC) was synthesized via facile pyrolysis of liquid precursors. Without any pre-treatment, put the 4 g of silicone oil into the alumina boat and place it in the furnace. The oil was pyrolyzed in Ar atmosphere, at 800 ^{o}C for 5 hrs with the heating rate of 5 ^{o}C min^{-1}. After heat treatment, cool down the product in the furnace to the room temperature and take out the sample. All materials were handled without any purification.

2.2 Preparation of S-SiOC

Mix 4 g of silicone oil and 800 mg of 1-dodecanethiol by using a mortar and pestle for sulfur doping. Subsequently, put the mixture into the alumina boat and place the boat in the tube furnace. And under the same condition with the SiOC, pyrolyze the mixture and take out the sample after cooling down to the room temperature.

2.3 Material characterization

The morphology analysis of samples was carried out with a field-emission scanning electron microscopy (FE-SEM, Hitachi S-4800)

and field-emission transmission electron microscopy (FE-TEM, JEOL JEM-F200) with an energy dispersive X-ray spectrometer (EDS). X-ray diffraction (XRD) patterns were obtained using a diffractometer (Bruker New D8-Advance) with Cu K_α radiation (λ = 1.5406 Å). X-ray photoelectron spectroscopy (XPS) analysis was conducted using an X-ray photoelectron spectrometer (KRATOS AXIS-HSi). Raman spectra were obtained using a Raman spectrometer (THERMO DXR2xi) with a 532 nm laser source.

2.4 Electrochemical measurements

The SiOC anode was fabricated by homogeneously mixing active materials, Super-P as a conductive material, and sodium carboxymethylcellulose (M_w ~90000, Sigma Aldrich) as a binder in a weight ratio of 70 : 15 : 15 in DI water using a Mini-Mill (PULVERISETTE 23 FRITSCH) for 30 minutes. Using a doctor blade, the mixture was spread onto a Cu foil and the electrode was dried at 60 ^oC in a vacuum oven for 4 hrs. The electrode was punched into a disk with a diameter of 11 mm. The mass loading of the active material was ~1.1 mg cm^{-2}. CR2016 Coin cells were assembled in an Ar-filled glovebox (O_2 and H_2O < 1 ppm). Cells

consisting of the S-SiOC as the anode, Li metal disk as the counter electrode and Celgard 2400 as the separator. 1.3 M $LiPF_6$ in a 3 : 7 (v/v) mixture of ethylene carbonate and diethyl carbonate with 10% fluoroethylene carbonate additive (PANAX) was used as an electrolyte. Cells were galvanostatically measured by using WBCS3000S cycler (WonAtech) at a voltage window of 0.01 and 3 V (*vs*. Li/Li^+). An electrochemical impedance spectroscopy (EIS) analysis was conducted using a ZIVE SP1 instrument in a frequency range between 100mHz and 100kHz. The electrical sheet resistance of electrodes was evaluated by four-point probe (CMT-100 MP, Advanced Instrument Technology).

3. Result and Discussion

3.1 Material analysis

The synthesis process of S-SiOC was presented in the schematic image (Fig. 1). Commercial silicone oil (polyphenyl-methylsiloxane) was used for precursor and 1-dodecanethiol was used as a source of sulfur. Since both silicone oil and 1-dodecanethiol are liquid, I simply mixed them up without any additional solvents or surfactants [12, 14] and the mixture was pyrolyzed at 800 ^{o}C in an Ar atmosphere. As a result, the black powders are obtained, which indicates the forming of carbon networks [11].

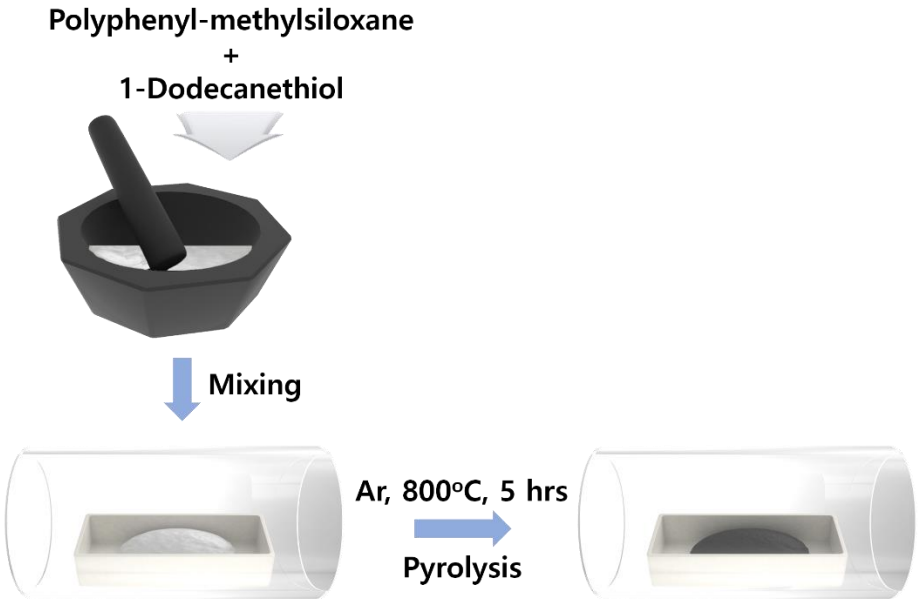

Figure 1. Schematic illustration of preparing the sulfur-doped silicon oxycarbide.

The morphology and the size of the particles are shown in the SEM images (Fig. 2). Particles in an irregular shape with various size distribution were observed in both samples. Both samples are mainly composed of relatively large particles in the range of 1-3 μm with relatively small particles. Large particles can improve the density and small particles can improve rate performance by increasing surface area. As shown in SEM images, doping sulfur makes no obvious differences in morphology between two samples.

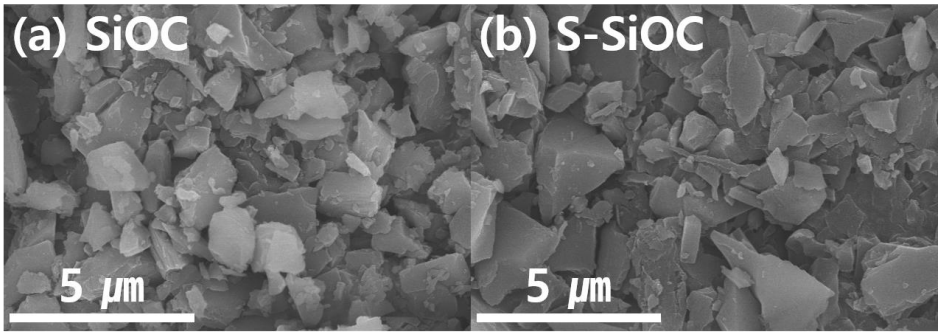

Figure 2. SEM images of (a) SiOC and (b) S-SiOC

X-ray diffraction (XRD) patterns of as-prepared SiOC and S-SiOC samples are shown in Fig. 3a. SiOC presented the broad diffraction peak at 2θ = ~23° which related to amorphous silica and the diffraction peak with the low intensity at 2θ = ~44°. Peaks of pristine sulfur were not detected, which confirms that S is not exist as an elemental state [38]. The broadness and the intensity of XRD patterns indicate that SiOC have amorphous structure as reported in previous works [14, 44-46]. Similar patterns were observed in S-SiOC which means that the doped sulfur atoms did not change the amorphous structure of SiOC. Besides, SiC crystallization was not detected because the pyrolysis temperature is not enough for carbothermal reduction [11, 47]. The absence of SiC is advantageous for enhanced reversible capacity because of its inaction for lithium ions [20]. The Raman spectra of both SiOC and S-SiOC are shown in Figure 3b. Two major peaks at 1330cm^{-1} and 1585cm^{-1} were observed, which are generally observed in carbonaceous

materials [34, 46-49]. The former peak is related to the D peak and the latter is associated with G peak respectively. The intensity ratio of the D and G peaks (I_D/I_G), which generally indicate disordering degree, apparently increased from 0.96 to 1.08 after sulfur doping. This result reflects the increase of defects in SiOC material due to doped-sulfur atoms. Because of the embedded graphene carbon layer into the amorphous Si-O-C phase and amorphous carbon phase, characteristic peaks of the graphitic carbon layer in the XRD were not observed despite of the existence of a G band in Raman spectra [11].

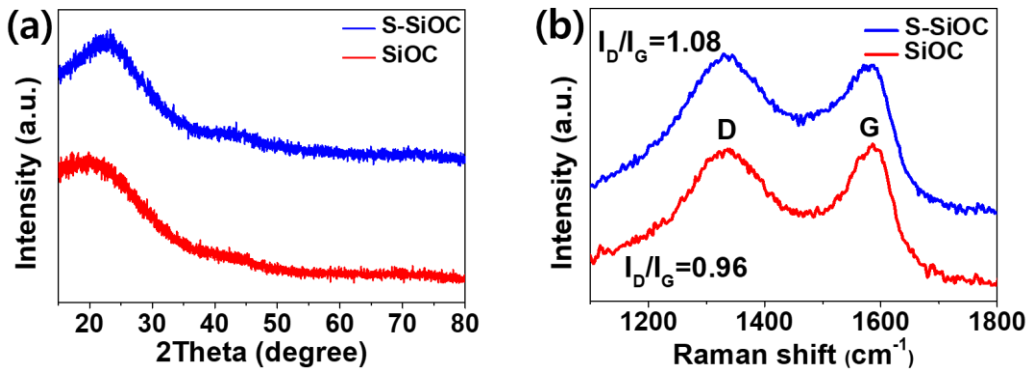

Figure 3. (a) XRD patterns of SiOC and S-SiOC. (b) Raman spectra of SiOC and S-SiOC.

For the further analysis of the morphology and the structure, TEM images of SiOC and S-SiOC with different magnifications were obtained in Fig. 4. In both samples, bulk particles with an irregular shape were observed as depicted in SEM images. Microstructures of SiOC (Fig. 4b) and S-SiOC (Fig. 4d) were obtained with HR-TEM images, which indicates that the sample has a completely amorphous structure without any crystallinity. The result verifies that the pyrolysis temperature was not enough for the formation of crystalline SiC and it is consistent with XRD patterns. Additionally, EDS elemental mapping was adopted for verifying the existence of Si, O, C, and S elements. It is clear that Si, O and C elements were well distributed and S was not contained in SiOC (Fig. 4e). However, S-SiOC presents a homogenous distribution of Si, O, C and S (Fig. 4f). EDS spectra of both samples were presented in Fig. 4g and Fig. 4h. In pure SiOC, there were peaks for Si, O, C at 1.74 keV, 0.53 keV and 0.28 keV respectively and no signal of S. In sulfur doped SiOC, however, all the peaks existed including a clear spectrum of the S at

about 2.31 keV (~ 3.11% in the atomic ratio). EDS elemental mapping images indicate that sulfur atoms were successfully doped into silicon oxycarbide.

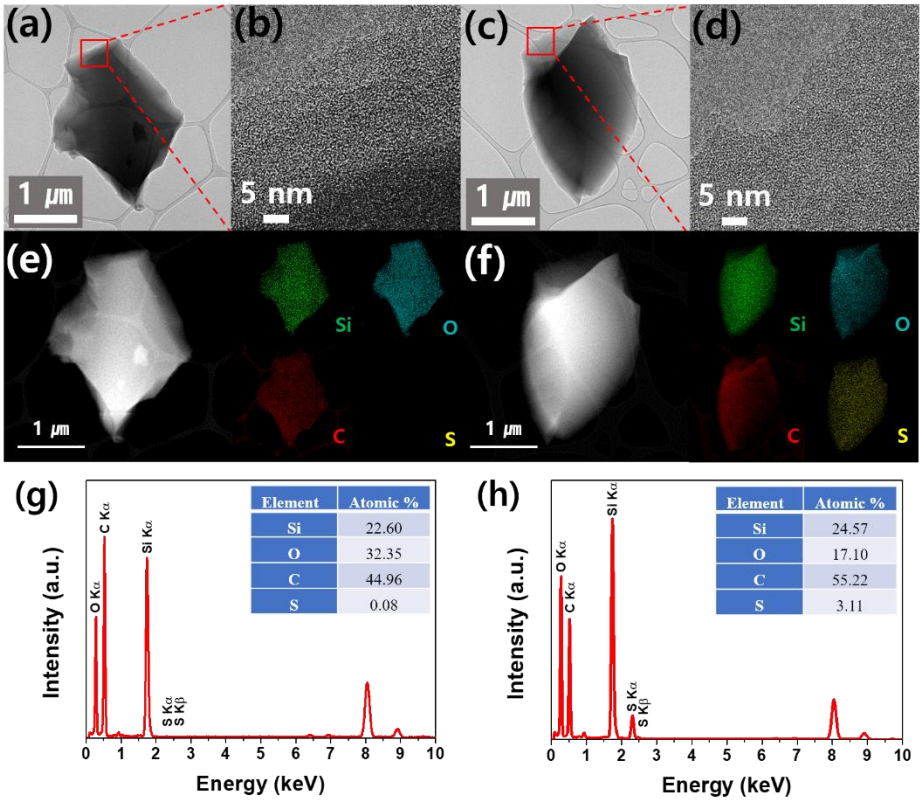

Figure 4. TEM and high resolution TEM images of (a), (b) SiOC and (c), (d) S-SiOC. EDS mapping of Si, O, C and S elements in (e) SiOC and (f) S-SiOC. Quantitative analysis spectra of (g) SiOC and (h) S-SiOC.

The surface chemical state of S-SiOC was characterized by X-ray photoelectron spectroscopy (XPS). Fig. 5 demonstrates high-resolution spectra of C 1s, O 1s, Si 2p, and S 2p in S-SiOC with the fitted results. The C 1s peak (Fig. 5a) was deconvoluted to six peaks of C-Si (283 eV), C=C (283.8 eV), C-C (284.4 eV), C-S (285.5 eV), C-O (286.5 eV), and C=O (288.3 eV). And the O 1s peak (Fig. 5b) was deconvoluted to four peaks of O-C (530 eV), O=C (531.2 eV), O-Si (531.7 eV), and Si-O-Si (532.4 eV). The C 1s spectrum in Fig. 5a, the peak intensity of C-C/C=C was increased in S-SiOC and C-S bonding peak was clearly observed, compared to SiOC (Fig. 6a). It can be inferred that doped sulfur atoms had some effects on the redistribution of Si-C and C-C/C=C bonds, changing the structure of both the Si-O-C glass phase and the free carbon phase. In the case of O 1s spectrum in Fig. 5b, O=C/O-C bonding peaks were decreased after doping. The results might be attributed to the fact that the O=C/O-C bonds were partially replaced by the C-S bonds. These substitutions can be beneficial for conductivity and enhanced electrochemical performances [37]. The Si 2p peak in Fig. 5c can be deconvoluted to four peaks of $SiOC_3$ (101.2 eV), SiO_2C_2 (102

eV), SiO_3C (102.5 eV), and SiO_4 (103.3 eV) as in previous works [11, 13, 50]. The differences of deconvoluted peaks were not changed significantly after S doping compared to bare SiOC (Fig. 6c). It can be also interpreted as the structural changes between two phases were occurred, without the formation of covalent bonds between silicon and sulfur atoms. The clear difference between the two samples was presented in the S 2p spectrum. The high-resolution S 2p spectrum for S-SiOC was consists of four peaks at 163.4 eV, 164.6 eV, 167.9 eV and 168.9 eV. The former two peaks with a splitting of 1.2 eV may be attributed to S $2p_{3/2}$ and S $2p_{1/2}$ for -C-S-C- bonding with a heterocyclic structure [32, 37, 38, 51]. The latter two peaks corresponded to oxidized sulfur groups [52]. These observations indicate that covalent bonds between sulfur and carbon atoms have been successfully formed [32, 49]. In SiOC, however, any visible peak did not exist in the S_{2p} spectrum.

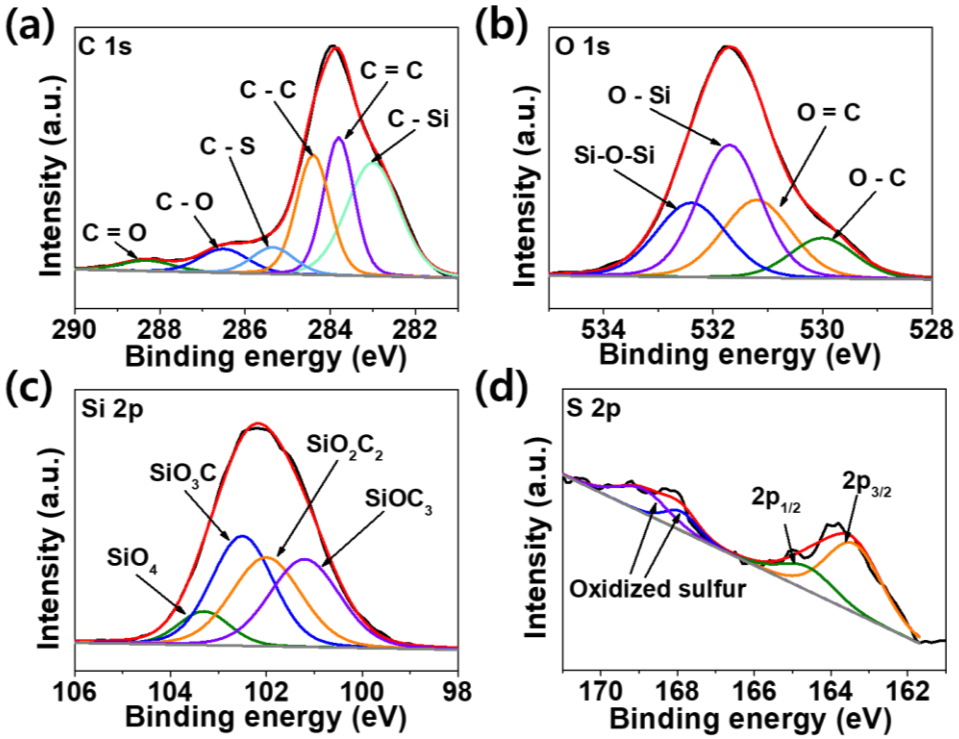

Figure 5. High resolution XPS spectra of (a) C 1s, (b) O 1s, (c) Si 2p and (d) S 2p in S-SiOC.

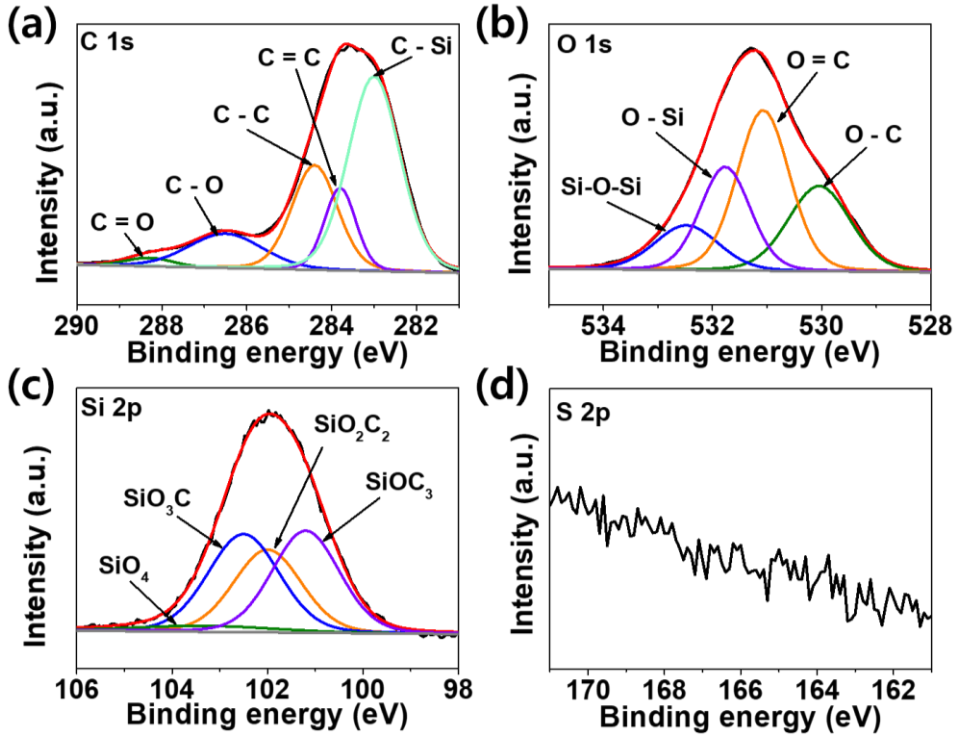

Figure 6. High resolution XPS spectra of (a) C 1s, (b) O 1s, (c) Si 2p and (d) S 2p in SiOC.

3.2 Electrochemical analysis

Cyclic voltammetry (CV) at a scan rate of 0.1 m V^{-1} was carried out for information about electrochemical reaction. CV curves for S-SiOC electrode (Fig. 7b) presented weak anodic peaks and sharp cathodic peaks at ca. 0.84 V and ca. 0.03 V (vs. Li^{+}/Li) respectively, which is typically obtained in SiOC-based materials [46, 53]. For SiOC electrode, similar CV curves were observed with weak anodic peaks at 0.87 V and sharp cathodic peaks at 0.01 V (Fig. 7a). In previous research about SiOC electrode, some irreversible peaks were shown at the voltage range of < 1.5 V which is related to lithium consumption by functional groups on the surface [54]. However, these peaks were not shown in this work, indicating that the functionalities on the surface of both samples can be neglected. The potential gap between anodic and cathodic peaks become narrower after sulfur doping, which infers that the polarization of the electrode was decreased. And the response current was increased in the S-SiOC electrode, which can be interpreted as the electrical conductivity was increased due to the doping process. Galvanostatic charging and discharging curves of both SiOC (Fig. 7c) and S-SiOC (Fig. 7d) were obtained for the initial 5 cycles at 1 A g^{-1} in the range of 0.01 – 3 V. For the initial cycle, the

discharging curve exhibits a plateau at ~0.8 V and no clear plateau was obtained, which is consistent with CV curves. Discharge capacities of SiOC and S-SiOC for the first cycle at 0.1 A g^{-1} are 1011 mAh g^{-1} and 1048 mAh g^{-1}, respectively. The reversible specific capacity of SiOC is 586 mAh g^{-1} with initial coulombic efficiency (ICE) of 58%. In the case of S-SiOC, a higher reversible capacity of 700 mAh g^{-1} and improved ICE of 66.8% were exhibited. The enhanced capacities of S-SiOC might be owing to the improved electrical conductivity by doping sulfur atoms [37]. The low ICE might be due to the irreversible side reaction which related to the electrolytes and irreversible lithiated products [20, 46]. The second discharge capacities of SiOC and S-SiOC are 513.6 mAh g^{-1} and 587.5 mAh g^{-1}, and the reversible specific capacities and coulombic efficiencies are 480.2 mAh g^{-1} with 93.4% and 610 mAh g^{-1} with 96.3%, respectively. The coulombic efficiencies tended to increase as the cycle proceeded.

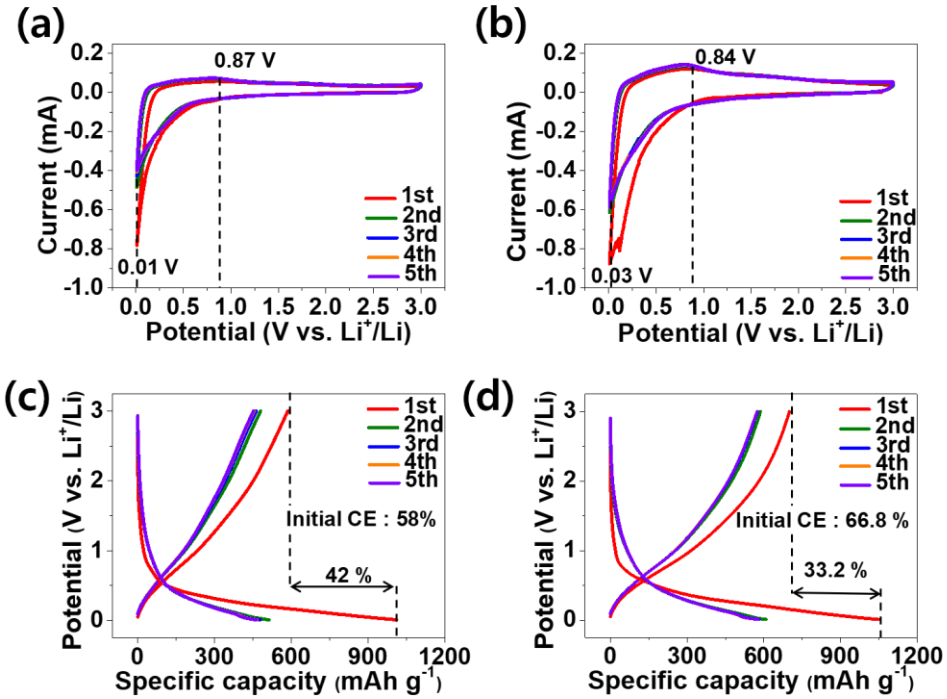

Figure 7. Cyclic voltammograms for the initial 5 cycles of (a) SiOC and (b) S-SiOC, at a scan rate of 0.1 m V s^{-1}. Galvanostatic profiles for the initial 5 cycles of (c) SiOC and (d) S-SiOC. The current density is 1 A g^{-1} except for the initial cycle of 0.1 A g^{-1}.

For the further investigation of doping effects on the electrochemical properties, CV curves with different scan rates for SiOC and S-SiOC were carried out (Fig. 8a and Fig. 8b, respectively). The scan rate was changed from 0.5 mV s^{-1} to 4 mV s^{-1}. As the scan rate increases, the peak current in both samples tends to increase. The result might be associated with the activation of the electrochemical reactions [46]. To examining the role of S doping for electrochemical performance, the linear relationship between the anodic peak current and the square root of the scan rate was observed in Fig. 8c. Peak A (shown in Fig. 8a) and Peak B (shown in Fig.8b) were used for SiOC and S-SiOC, respectively. D_{Li}, the diffusion coefficient of lithium ion, were calculated from the CV curves with different scan rate by Randles-Sevcik equation,

$$\mathrm{I}_p = 2.69 \times 10^5 n^{1.5} A {D_{Li}}^{0.5} v^{0.5} C_{Li}$$

where I_p is the peak current, A is the area of the anode, n is the number of electrons in the corresponding reaction, v is the

scan rate, C_{Li} is the lithium ions concentration in the electrolyte [55, 56]. From these plots and the equation, the slope was calculated to be 8.67×10^{-4} for SiOC and 1.22×10^{-3} for S-SiOC. The calculated value for S-SiOC was larger than that of SiOC, which indicates the doping sulfur can strongly improve the electrochemical kinetics of Li^+ [57, 58].

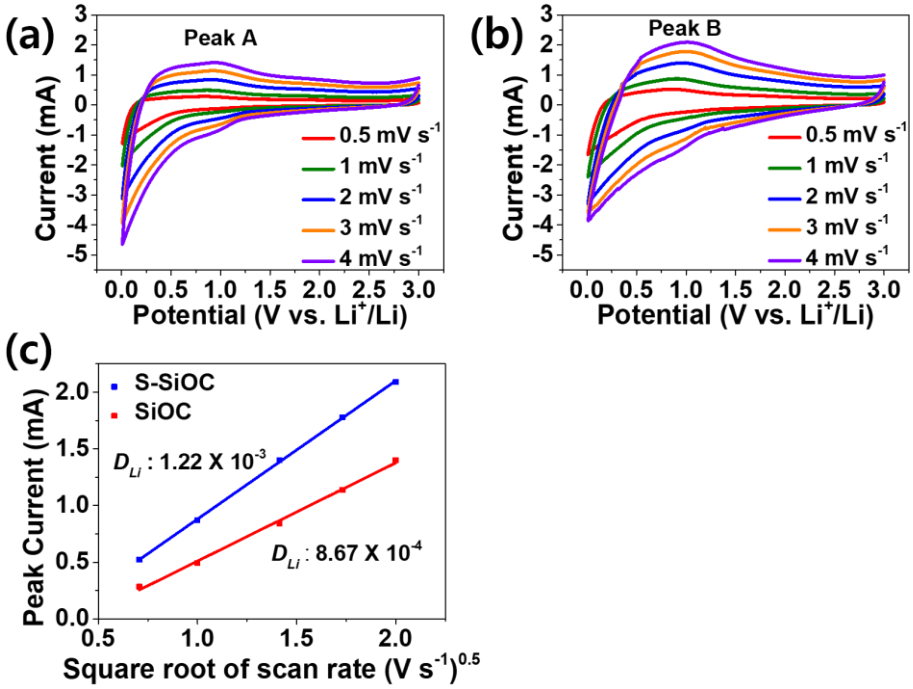

Figure 8. CV curves with different scan rates from 0.5 mV s^{-1} to 4 mV s^{-1} of (a) SiOC and (b) S-SiOC. (c) Corresponding variation of the anodic peak current (A, B) from 8a, 8b with the square root of the scan rate.

Next, electrochemical impedance spectroscopy (EIS) was carried out to understand the enhanced electrochemical kinetics of S-doped SiOC electrodes before cycling. All the half-cells were fabricated as symmetric cells for neglecting the effects of Li metal. The Nyquist plots of electrodes were shown in Fig. 9a, with the inset of magnified in high-frequency region. The intercept of X-axis with the curve and the semicircle corresponds to the value of interfacial resistance and the charge transfer resistance, respectively, at the interface between the electrolyte and electrode [36, 59]. As shown in the inset, the intercept of X-axis with the curve is clearly reduced after S doping. S-SiOC presents interfacial resistance of ~ 4.2 Ω, which is much lower than that of SiOC (~ 8.4 Ω). And the charge transfer resistance of the S-SiOC electrode (~ 20.8 Ω) was significantly reduced compared to the SiOC electrode (~ 96.4 Ω), evaluated based on the semicircle in the high-middle frequency regions. Thus, EIS characteristics inferred that S doping can improve the electrical

conductivity and enhance the rate capability of the electrode. The rate performance of SiOC and S-SiOC was measured with different current densities, as shown in Fig. 9b. The SiOC electrodes deliver reversible specific capacities of 455, 353, 295, 213 and 109 mAh g^{-1} at 0.2, 0.5, 1, 2 and 4 A g^{-1}, respectively. Due to the enhanced electrical conductivity, S-SiOC electrodes deliver much higher capacities of 580, 453, 371, 292 and 200 mAh g^{-1} at 0.2, 0.5, 1, 2 and 4 A g^{-1}, respectively. The larger reversible specific capacities of 465 mAh g^{-1} and 612 mAh g^{-1} were obtained for SiOC and S-SiOC, respectively, with turning back of the current density from 4 A g^{-1} to 0.2 A g^{-1}. These results may be owing to the activation of electrodes during cycling. The cycling performances of electrodes were evaluated at 1 A g^{-1}, as shown in Fig. 9c. Both SiOC and S-SiOC electrodes exhibit outstanding cycling stability with almost no capacity decay because of the structural stability in the SiOC-based electrode [7]. After 1000 cycles, the high coulombic

efficiencies of 99.8% were observed in both electrodes. However, S-SiOC shows a higher specific capacity of 378 mAh g^{-1} with an excellent capacity retention of 84.9% than SiOC, which has the specific capacity 270 mAh g^{-1} with a capacity retention of 70.3%.

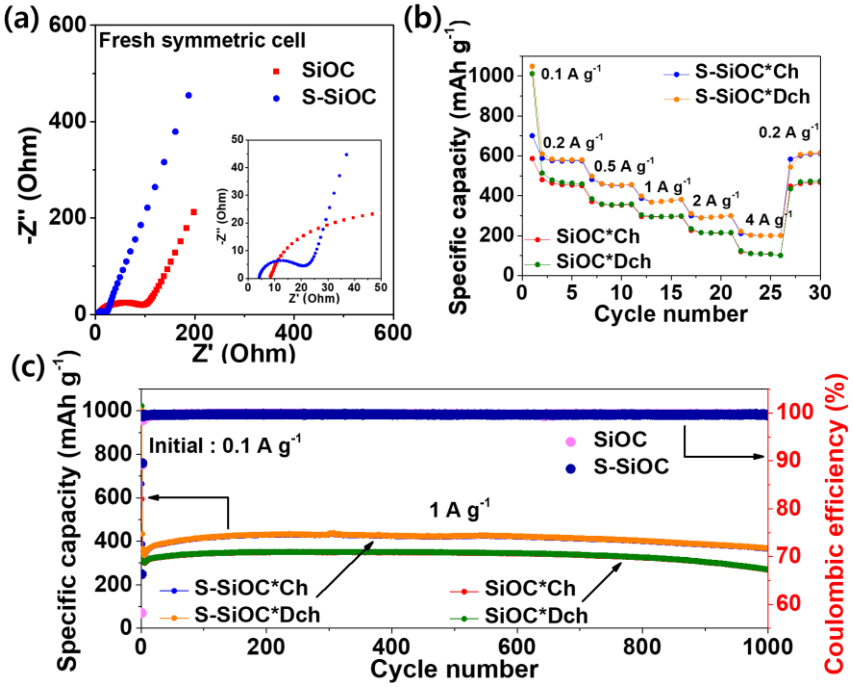

Figure 9. (a) Nyquist plots of SiOC and S-SiOC electrodes for fresh symmetric cells. (b) Rate performance of SiOC and S-SiOC at different current densities. (c) Cycling performance and initial coulombic efficiency of SiOC and S-SiOC at 1 A g^{-1} for 1000 cycles.

To find out the beneficial feature of S doping for the electrical conductivity, I additionally measured the sheet resistance of the SiOC and S-SiOC electrodes (Fig. 10). The sheet resistance was measured for 400 times in both electrodes, and the average value and the standard deviation of the sheet resistance were noted. The measured average sheet resistance and the deviation of S-SiOC electrodes were 157.34 Ω $\square^{-1}$ with a deviation of 10.54 Ω $\square^{-1}$. For SiOC electrodes, however, they exhibit the average sheet resistance of 228.98 $\square^{-1}$ with a deviation of 20.16 $\square^{-1}$, which was much larger than that of S-SiOC electrodes. Thus, the increased electrical conductivity of the S-SiOC electrode can also be said to the effect of doping and the reduced polarization in CV curves can be explained by these results. These electrochemical results match well with the previous assumption, improved conductivity due to the S doping.

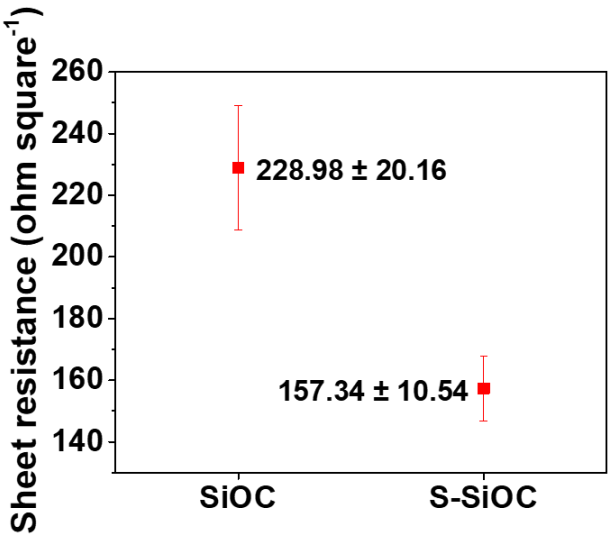

Figure 10. Sheet resistance of the SiOC and S-SiOC electrodes.

4. Conclusion

Sulfur-doped silicon oxycarbide (S-SiOC) was successfully synthesized via the facile pyrolysis process of a commercial silicone oil. In this work, I have demonstrated its outstanding performances as an anode material for LIBs. The experimental evidences proved that introducing S atoms increased Li^+ storage capacity and the rate capability by accelerating Li^+ diffusion. Moreover, electrical conductivity of the material was improved due to the formation of covalent bonds between carbon and sulfur atoms. Even after the 1000^{th} cycle, the electrode shows a specific capacity of 378 mAh g^{-1} with high a capacity retention of 84.8%. In the future works, the performances can be enhanced by examining the doping mechanism and the structure of materials. Therefore, as an anode material in LIBs, introducing dopants into silicon oxycarbide can be an effective way to obtain better electrochemical performance.

References

[1] J.-M. Tarascon and M. Armand, Issues and challenges facing rechargeable lithium batteries, *Nature*, 2001, *414*, 359-367.

[2] P. G. Bruce, B. Scrosati and J.-M Tarascon, Nanomaterials for rechargeable lithium batteries, Angew. Chem. Int. Ed., 2008, 47, 2903-2946.

[3] J. B. Goodenough and Y. Kim, Challenges for rechargeable Li batteries, Chem. Mat., 2010, 22, 587-603.

[4] N. Nitta, F. Wu, J. T. Lee and G. Yushin, Li-ion battery materials: present and future, Mater. Today, 2015, 18, 252-264.

[5] H. Fukui, Y. Harimoto, M. Akasaka and K. Eguchi, Lithium species in electrochemically lithiated and delithiated silicon oxycarbides, ACS Appl. Mater. Interfaces, 2014, 6, 12827-12836.

[6] C. K. Chan, H. Peng, G. Liu, K. Mcllwrath, X. F. Zhang, R. A. Huggins and Y. Cui, High-performance lithium battery anodes using silicon nanowires, Nano Lett., 2011, 11, 2949-2954.

[7] Y. Yao, M. T. McDowell, I. Ryu, H. Wu, N. Liu, L. Hu, W. D. Nix and Y. Cui, Interconnected silicon hollow nanospheres for lithium-ion battery anodes with long cycle life, Nano Lett., 2011, 11, 2949-2954.

[8] H. Kim and J. Cho, Superior lithium electroactive mesoporous Si@carbon core-shell nanowires for lithium battery anode material, Nano Lett., 2008, 8, 3688-3691.

[9] H. Sun and K. Zhao, Atomistic origins of high capacity and high structural stability of polymer-derived SiOC anode materials, ACS Appl. Mater. Interfaces, 2017, 9, 35001-35009.

[10] M. Graczyk-Zajac, L. M. Reinold, J. Kaspar, P. V. W. Sasikumar, G. D. Soraru and R. Riedel, New insights into understanding irreversible and reversible lithium storage within SiOC and SiCN ceramics, Nanomater., 2015, 5, 233-245.

[11] C. Chandra and J. Kim, Silicon oxycarbide produces from silicone oil for high-performance anode material in sodium ion batteries, Chem. Eng. J., 2018, 338, 126-136.

[12] Y. Lee, K. Y. Lee and W. Choi, One-pot synthesis of antimony-embedded silicon oxycarbide materials for high-performance sodium-ion batteries, Adv. Funct. Mater., 2017, 27, 1702607.

[13] M. Halim, C. Hudaya, A. Y. Kim and J. K. Lee, Phenyl-rich silicone oil as a precursor for SiOC anode materials in long-cycle and high-rate lithium ion batteries, J. Mater. Chem. A, 2016, 4, 2651-2656.

[14] D. Kim, H. Kim, H. Lim, K. J. Kim, H. G. Jung, D. Byun, C. Kim and W. Choi, A facile control in free-carbon domain with divinylbenzene for the high-rate-performing Sb/SiOC composite anode material in sodium-ion batteries, Int. J. Energy Res., 2020, 44, 11473-11486.

[15] R. J.-C. Dubey, P. V. W. Sasikumar, N. Cerboni, M. Aebli, F. Krumeich, G. Blugan, K. V. Kravchyk, T. Graule and M. V. Kovalenko, Silicon oxycarbide-antimony nanocomposites for high-performance Li-ion battery anodes, Nanoscale, 2020, 12, 13540-13547.

[16] C. Chandra, H. S. Cahyadi, S. Alvin, W. Devina, J.-H. Park, W. Chang, K. Y. Chung, S. K. Kwak and J. Kim, Revealing the sodium storage mechanism in high-temperature-synthesized silicon oxycarbides, Chem. Mater., 2020, 32, 410-423.

[17] A. M. Wilson, J. N. Reimers, E. W. Fuller and J. R. Dahn, Lithium insertion in pyrolyzed siloxane polymer, Solid State Ionics, 1994, 74, 249-254.

[18] A. M. Wilson, G. Zank, K. Eguchi, W. Xing, B. Yates and J. R. Dahn, Polysiloxane pyrolysis, Chem. Mater., 1997, 9, 1601-1606.

[19] W. Xing, A. M. Wilson, K. Eguchi, G. Zank and J. R. Dahn,

Pyrolyzed polysiloxanes for use as anode materials in lithium-ion batteries, J. Electrochem. Soc., 1997, 144, 2410-2416.

[20] X. Liu, M.-C. Zheng and K. Xie, Mechanism of lithium storage in Si-O-C composite anodes, J. Power Sources, 2011, 196, 10667-10672.

[21] R. Bhandavat and G. Singh, Stable and efficient Li-ion battery anodes prepared from polymer-derived silicon oxycarbide-carbon nanotube shell/core composites J. Phys. Chem. C, 2013, 117, 11899-11905.

[22] G. Shao, D. A. H. Hanaor, J. Wang, D. Kober, S. Li, X. Wang, X. Shen, M. F. Bekheet and A. Gurlo, Polymer-derived SiOC integrated with a graphene aerogel as a highly stable Li-ion battery anode, ACS Appl. Mater. Interfaces, 2020, 12, 46045-46056.

[23] R. Bhandavat, M. Cologna and G. Singh, Polymer-derived SiOC-CNT paper as lithium-ion battery anodes, Nanomaterials and Energy, 2012, 1, 57-61.

[24] Y. Li, Y. Hu, Y. Lu, S. Zhang, G. Xu, K. Fu, S. Li, C. Chen, L. Zhou, X. Xia and X. Zhang, One-dimensional SiOC/C composite nanofibers as binder-free anodes for lithium-ion batteries, J.

Power Sources, 2014, 254, 33-38.

[25] L. David, R. Bhandavat, U. Barrera and G. Singh, Silicon oxycarbide glass-graphene composite paper electrode for long-cycle lithium-ion batteries, Nat. Commun., 2016, 7, 10998.

[26] Y. Ren, B. Yang, X. Huang, F. Chu, J. Qiu and J. Ding, Intercalated SiOC/graphene composites as anode material for Li-ion batteries, Solid State Ionics, 2015, 278, 198-202.

[27] Z. Sang, X. Yan, L. Wen, D. Su, Z. Zhao, Y. Liu, H. Ji, J. Liang and S. X. Dou, A graphene-modified flexible SiOC ceramic cloth for high-performance lithium storage, Energy Storage Mater., 2020, 25, 876-884.

[28] R. J.-C. Dubey, P. V. W. Sasikumar, F. Krumeich, G. Blugan, J. Kuebler, K. V. Kravchyk, T. Graule and M. V. Kovalenko, Silicon oxycarbide-tin nanocompsite as a high-power-density anode for Li-ion batteries, Adv. Sci., 2019, 6, 1901220.

[29] J. Kaspar, C. Terzioglu, E. Ionescu, M. Graczyk-Zajac, S. Hapis, H.-J. Kleebe and R. Riedel, Stable SiOC/Sn nanocomposite anodes for lithium-ion batteries with outstanding cycling stability, Adv. Funct. Mater., 2014, 24, 4097-4104.

[30] J. Wang, R. Ma, Z. Zhou, G. Liu and Q. Liu, Magnesiothermic

synthesis of sulfur-doped graphene as an efficient metla-free electrocatalyst for oxygen reduction, Sci. Rep., 2015, 5, 9304.

[31] C. Hu, D. Liu, Y. Xiao and L. Dai, Functionalization of graphene materials by heteroatom-doping for energy conversion and storage, Prog. Nat. Sci., 2018, 28, 121-132.

[32] B. Quan, A. Jin, S.-H. Yu, S. M. Kang, J. Jeong, H. D. Abruna, L. Jin, Y. Piao and Y.-E. Sung, Solvothermal-derived S-doped graphene as an anode material for sodium-ion batteries, Adv. Sci., 2018, 5, 1700880.

[33] Y. Yang, S. Jin, Z. Zhang, Z. Du, H. Liu, J. Yang, H. Xu and H. Ji, Nitrogen-doped hollow carbon nanospheres for high-performance Li-ion batteries, ACS Appl. Mater. Interfaces, 2017, 9, 14180-14186.

[34] Y. Tan, C. Xu, G. Chen, Z. Liu, M. Ma, Q. Xie, N. Zheng and S. Yao, Synthesis of ultrathin nitrogen-doped graphitic carbon nanocages as advanced electrode materials for supercapacitor, ACS Appl. Mater. Interfaces, 2013, 5, 2241-2248.

[35] X. Miao, D. Sun, X. Zhou and Z. Lei, Designed formation of nitrogen and sulfur dual-doped hierarchically porous carbon for long-life lithium and sodium ion batteries, Chem. Eng. J., 2019,

364, 208-216.

[36] J. Lin, Y. Xu, J. Wang, B. Zhang, D. Li, C. Wang, Y. Jin and J. Zhu, Nitrogen-doped hierarchically porous carbonaceous nanotubes for lithium ion batteries, Chem. Eng. J., 2018, 352, 964-971.

[37] X. Zhou, Z. Zhang, P. Yan, Y. Jiang, H. Wang and Y. Tang, Sulfur-doped reduced graphene oxide/Sb_2S_3 composite for superior lithium and sodium storage, Mater. Chem. Phys., 2020, 244, 122661.

[38] X. Wang, G. Li, F. M. Hassan, J. Li, X. Fan, R. Batmaz, X. Xiao and Z. Chen, Sulfur covalently bonded graphene with large capacity and high rate for high-performance sodium-ion batteries anodes, Nano Energy, 2015, 15, 746-754.

[39] J. P. Paraknowitsch and A. Thomas, Doping carbons beyond nitrogen: an overview of advanced heteroatom doped carbons with boron, sulphur and phosphorus for energy applications, Energy Environ. Sci., 2013, 6, 2839-2855.

[40] Q. Hu, Y. Meng, H. Zhang, G. Zhao, J. Hu, F. Zhu and Y. Zhang, Encapsulated Ni_3S_2 nanoparticles with N, S dual-doped carbon nanotubes: A robust structure for lithium storage, J. Electroanal.

Chem., 2020, 873, 114383.

[41] H. Tao, M. Zhou, K. Wang, S. Cheng and K. Jiang, Nickel sulfide nanospheres anchored on reduced graphene oxide *in situ* doped with sulfur as a high performance anode for sodium-ion batteries, J. Mater. Chem. A, 2017, 5, 9322-9328.

[42] C. H. A. Wong, Z. Sofer, K. Klimova and M. Pumera, Microwave exfoliation of graphite oxide in H_2S plasma for the synthesis of sulfur-doped graphenes as oxygen reduction catalysts, ACS Appl. Mater. Interfaces, 2016, 8, 31849-31855.

[43] H. L. Poh, P. Simek, Z. Sofer and M. Pumera, Sulfur-doped graphene *via* thermal exfoliation of graphite oxide in H_2S, SO_2, or CS_2 gas, ACS Nano, 2013, 7, 5262-5272.

[44] M. Wang, Y. Xia, X. Wang, Y. Xiao, R. Liu, Q. Wu, B. Qiu, E. Metwalli, S. Xia, Y. Yao, G. Chen, Y. Liu, Z. Liu, J.-Q. Meng, Z. Yang, L.-D. Sun, C.-H. Yan, P. Muller-Buschbaum, J. Pan and Y.-J. Cheng, Silicon oxycarbide/carbon nanohybrids with tiny silicon oxycarbide particles embedded in free carbon matrix based on photoactive dental methacrylaates, ACS Appl. Mater. Interfaces, 2016, 8, 13982-13992.

[45] H. Fukui, H. Ohsuka, T. Hino and K. Kanamura, A Si-O-C

composite anode: High capability and proposed mechanism of lithium storage associated with microstructural characteristics, ACS Appl. Mater. Interfaces, 2010, 2, 998-1008.

[46] H. Shi, A. Yuan and J. Xu, Tailored synthesis of monodispersed nano/submicron porous silicon oxycarbide (SiOC) spheres with improved Li-storage performance as an anode material for Li-ion batteries, J. Power Sources, 2017, 364, 288-298.

[47] J. Kaspar, M. Graczyk-Zajac and R. Riedel, Lithium insertion into carbon-rich SiOC ceramics: Influence of pyrolysis temperature on electrochemical properties, J. Power Sources, 2013, 244, 450-455.

[48] Z. Li, Z. Xu, X. Tan, H. Wang, C. M. B. Holt, T. Stephenson, B. C. Olsen and D. Mitlin, Mesoporous nitrogen-rich carbons derived from protein for ultra-high capacity battery anodes and supercapacitors, Energy Environ. Sci., 2013, 6, 871-878.

[49] J. Yang, X. Zhou, D. Wu, X. Zhao and Z. Zhou, S-doped N-rich carbon nanosheets with expanded interlayer distance as anode materials for sodium-ion batteries, Adv. Mater., 2017, 29, 1604108.

[50] S. Yu, R. Tu and T. Goto, Preparation of SiOC nanocomposite

films by laser chemical vapor deposition, J. Eur. Ceram. Soc., 2016, 36, 403-409.

[51] L. Qie, W. Chen, X. Xiong, C. Hu, F. Zou, P. Hu and Y. Huang, Sulfur-doped carbon with enlarged interlayer distance as a high-performance anode material for sodium-ion batteries, Adv. Sci., 2015, 2, 1500195.

[52] X. Yu and H. S. Park, Sulfur-incorporated, porous graphene films for high performance flexible electrochemical capacitors, Carbon, 2014, 77, 59-65.

[53] M. Wilamowska-Zawlocka, P. Puczkarski, Z. Grabowska, J. Kaspar, M. Graczyk-Zajac, R. Riedel and G. D. Sorarù, Silicon oxycarbide ceramics as anodes for lithium ion batteries: influence of carbon content on lithum storage capacity, RSC Adv., 2016, 6, 104597-104607.

[54] M. Ma, H. Wang, M. Niu, L. Su, X. Fan, J. Deng, Y. Zhang and X. Du, High rate capabilities of HF-etched SiOC anode materials derived from polymer for lithium-ion batteries, RSC Adv., 2016, 6, 43316-43321.

[55] H. Kim, J. Lee, H. Ahn, O. Kim and M. J. Park, Synthesis of three-dimensionally interconnected sulfur-rich polymers for

cathode materials of high-rate lithium-sulfur batteries, Nat. Commun., 2015, 6, 7278.

[56] H. Li, Z. Cheng, A. Natan, A. M. Hafez, D. Cao, Y. Yang and H. Zhu, Dual-function, tunable, nitrogen-doped carbon for high-performance Li metal-sulfur full cell, Small, 2019, 15, 1804609

[57] C.-W. Chang-Jian, B.-C. Ho, C.-K. Chung, J.-A. Chou, C.-L. Chung, J.-H. Huang, J.-H. Huang and Y.-S. Hsiao, Doping and surface modification enhance the applicability of $Li_4Ti_5O_{12}$ microspheres as high-rate anode materials for lithium ion batteries, Ceram. Int., 2018, 44, 23063-23072.

[58] J.-Y. Lin, C.-C. Hsu, H.-P. Ho and S.-h. Wu, Sol-gel synthesis of aluminum doped lithium titanate anode material for lithium ion batteries, Electrochim. Acta, 2013, 87, 126-132.

[59] M. A. Abass, A. A. Syed, C. Gervais and G. Singh, Synthesis and electrochemical performance of a polymer-derived silicon oxycarbide/boron nitride nanotube composite, RSC Adv., 2017, 7, 21576-21584.

국 문 초 록

실리콘 옥시카바이드는 우수한 사이클 수명과 Si, O, C 원자들의 결합들로 이루어진 독특한 구조로 인해 리튬이온전지의 새로운 음극물질로 주목받고 있다. 그러나 실리콘 옥시카바이드 기반의 음극물질은 낮은 전기전도성이라는 단점을 가지고 있다. 본 연구에서는 상용화된 실리콘 오일과 도데칸사이올을 섞어 간단한 열분해 과정을 통해 황이 도핑된 실리콘옥시카바이드를 합성하고 이를 리튬이온전지의 음극 물질로 활용하는 연구를 진행하였다. 황 도핑을 통해 전기전도성을 향상시키고 추가적인 반응 지역을 만들어 더 많은 리튬이온을 저장시킬 수 있었고, Randles-Sevcik 방정식을 통해 향상된 전기화학적 성능을 확인하였다. 결과적으로, 합성된 황 도핑된 실리콘옥시카바이드는 초기 사이클에서 높은 가역용량 (0.1 A g^{-1}에서 700 mAh g^{-1})과 좋은 사이클 수명 특성 (1 A g^{-1}에서 1000회 충·방전 후, 378 mAh g^{-1}의 가역용량)을 보인다.

주요어: 실리콘 옥시카바이드, 황 도핑, 음극 물질, 리튬이온전지

학 번: 2019-27948